Atmos. Meas. Tech. Discuss., 7, 4275–4319, 2014
www.atmos-meas-tech-discuss.net/7/4275/2014/
doi:10.5194/amtd-7-4275-2014


Atmospheric Measurement Techniques Discussions



# Mixing layer height retrieval with ceilometer and Doppler lidar: from case studies to long-term assessment

**J. H. Schween**[1], **A. Hirsikko**[2], **U. Löhnert**[1], **and S. Crewell**[1]

[1]Inst. f. Geophysics and Meteorology, Univ. of Cologne, Cologne, Germany
[2]Forschungszentrum Jülich GmbH, Institut für Energie-und Klimaforschung: Troposphäre (IEK-8), Jülich, Germany

Received: 14 February 2014 – Accepted: 11 April 2014 – Published: 30 April 2014

Correspondence to: J. H. Schween (jschween@uni-koeln.de)

Published by Copernicus Publications on behalf of the European Geosciences Union.







## Abstract

Aerosol signatures observed by ceilometers are frequently used to derive mixing layer height (MLH) which is an essential variable for air quality modeling. Doppler wind lidar measurements of vertical velocity can provide a more direct estimation of MLH via simple thresholding. A case study reveals difficulties in the aerosol based MLH retrieval during transition times when the mixing layer is built up in the morning and when turbulence decays in the afternoon. The differences can be explained by the fact that the aerosol distribution is related to the history of the mixing process and aerosol characteristics are modified by humidification. The results of the case study are generalized by evaluating one year of joint measurements by a Vaisala CT25K and a HALO Photonics Streamline wind lidar. On average the aerosol based retrieval gives higher MLH than the wind lidar with an overestimation of MLH by about 300 m (600 m) in the morning (late afternoon). When turbulence is fully developed around noon best agreement is found between both methods. This diurnal behavior is even more pronounced in fair weather conditions classified by less than 4 octa. In these conditions the mean diurnal cycle of cloud base height corresponds well to the mixing layer height showing potential for a simplified MLH estimation.

## 1 Introduction

The atmospheric boundary layer (American Meteorological Society, 2013, http://glossary.ametsoc.org/wiki/Atmospheric_boundary_layer) is the lowest part of the atmosphere that is in contact with the Earth's surface (American Meteorological Society, 2014). The mixed layer (http://glossary.ametsoc.org/wiki/Mixing_layer) is a type of ABL where exchange processes between the Earth's surface and the atmosphere occur via turbulent mixing (see e.g. Oke, 1987; American Meteorological Society, 2014). Gaseous and particulate constituents emitted from the surface become well mixed within the ML which is capped by a temperature inversion or statically stable layer of





AMTD
7, 4275–4319, 2014



air. Therefore, aerosol particle concentration is high in the mixed layer whereas further up in the free troposphere aerosol concentrations are generally much lower. Atmospheric pollutants are dispersed within the ML and thus, mixed layer height (MLH) is an important parameter for air quality applications. Any model that attempts to predict concentrations needs MLH as a parameter or must be able to describe its evolution (e.g. Collier et al., 2005; White et al., 2009). Furthermore, the MLH determines if cumulus clouds can develop depending on whether the convective condensation level is reached making it a relevant quantity for numerical weather prediction.

Daytime ABL turbulent mixing is driven by solar radiation energy, which – to a major part – is absorbed by the Earth's surface and re-emitted to the atmosphere in form of long-wave terrestrial radiation and turbulent fluxes of latent and sensible heat (i.e. convection, Stull, 1988; Garratt, 1994). The formation of clouds reduces the incoming solar radiation at the surface and thus the turbulent heat fluxes from the surface into the atmosphere. This introduces a feedback mechanism modulating the exchange between surface and atmosphere. After sunset on days with strong local and weak synoptical forcing, convection decays and a neutral or slightly stable nocturnal ABL forms, called residual layer (http://glossary.ametsoc.org/wiki/Residual_layer). At night the emission of long-wave radiation by the surface leads to strong cooling and the formation of a stable nocturnal boundary layer (http://glossary.ametsoc.org/wiki/Nocturnal_boundary_layer) close to the surface. In low wind speed situations stratification of the NBL can be very strong leading to a decoupling of the layer above and as a consequence to the formation of the so-called nocturnal low level jet (NLLJ) (Garratt, 1994) which may induce intermittent turbulent mixing (Banta et al., 2006). In case of moderate surface winds a shallow nocturnal mixing layer may be formed induced by surface roughness and stored heat (Souch and Grimmond, 2006).

A number of methods exist to determine the MLH from different measurements (Seibert et al., 2000). Most of them are based on proxies, such as temperature, humidity or Richardson number, for the mixing process. These parameters are used in radiosonde based retrievals which are often considered to be the most reliable as they





AMTD
7, 4275–4319, 2014



are based on in-situ measured parameters, and are therefore used as reference in several studies (e.g. Eresmaa et al., 2006; Sicard et al., 2006; Münkel et al., 2007; O'Connor et al., 2010). However, determination of the MLH from radiosonde data is not that straightforward because no unambiguous separation between ML and the atmosphere above might be found (Seibert et al., 2000). Additionally, radiosondes measure properties along their flight path and their data might not be representative for the atmospheric column above the measurement site. Due to the fact that a radiosonde follows the horizontal wind during its ascent, it tends to move into regions with convergence and avoids regions with divergence. As a result radiosonde profiles are in convective situations biased towards properties of rising plumes.

The main shortcoming of radiosondes for MLH estimation is their coarse temporal resolution. This can be overcome by continuously operating ground based remote sensing instruments. Lidar (Light Detection and Ranging) systems have been used for atmospheric research since the 1960s (Weitkamp, 2005). An aerosol lidar determines the aerosol backscatter coefficient $\beta$ which depends on number concentration, size and optical properties of the aerosol particles. Assuming that the main source for aerosol and its precursors is at the surface turbulent mixing will lead to a uniform high aerosol concentration in the ML and a distinct gradient to much lower concentrations in the atmosphere above. Thus it should be possible to derive MLH from lidar by using the aerosol backscatter as a proxy. A number of different remote sensing based algorithms exist to detect MLH (see e.g. Emeis et al., 2008). They are based on evaluating the gradient of the backscatter profile (Endlich et al., 1979), its logarithm (Senff et al., 1996), fitting to a function (Steyn et al., 1999; Eresmaa et al., 2012) or application of the Haar wavelet analysis (Davis et al., 2000; Brooks, 2003; Haij et al., 2006). Even though advantages and disadvantages of different methods have been investigated by several studies (see e.g. Sicard et al., 2006; Haij et al., 2007; Eresmaa et al., 2012; Haeffelin et al., 2012)

Lidar ceilometers are robust low power, low cost and low maintenance lidars designed to determine the cloud base height (ceiling) but also provide the backscatter





AMTD
7, 4275–4319, 2014



profile, though with less sensitivity than a lidar. Several studies have proposed that ceilometer measured backscatter profiles can be used to derive the MLH (e.g. Münkel et al., 2007; Eresmaa et al., 2006, 2012). Many airports have operational ceilometers, and therefore, attempts are made to use them for a network of MLH observations (Haeffelin et al., 2012).

Doppler lidars offer a more direct approach to investigate the ABL mixing (e.g. Cohn and Angevine, 2000; Hogan et al., 2009). Instead of measuring a proxy for the vertical mixing, Doppler lidars measure directly the vertical air velocity. Engineering progress but also growth of the wind energy industry in the last two decades have led to the development of affordable and robust Doppler lidar systems (e.g. Pearson et al., 2010). MLH can be estimated by using a threshold value for the vertical velocity standard deviation $\sigma_w$ (e.g Tucker et al., 2009; Pearson et al., 2010; Barlow et al., 2011; Träumner et al., 2011). Another method is to use turbulent energy dissipation rate as proposed by O'Connor et al. (2010). This method is based on the assumption that measurements take place in the inertial subrange. However, the effort to ensure this is rather high (investigation of turbulent spectra) and reduces the universality of the method. Träumner et al. (2011) discuss several methods based on the semi-theoretical $\sigma_w$ profile as proposed by Lenschow et al. (1980). They find that the use of a threshold for $\sigma_w$ is the most robust method. Martucci et al. (2012) propose a yet different approach. The MLH is located at the level of a distinct negative gradient in the $\sigma_w$ profile. This is somehow a contradiction to the semi-theoretical profiles which show a smooth decay with more or less constant gradients towards the top of the ML (Lenschow et al., 1980; Sorbjan, 1989).

Currently, only relatively few comparisons of MLH retrievals between aerosol and Doppler lidars exist. A qualitative comparison of Doppler lidar derived vertical wind speed and MLH derived from aerosol backscatter profiles was performed by Baars et al. (2008) for a time period of three days. They find that aerosol based MLH retrievals agree with the height of the layer within which the largest vertical wind speeds occur. Tucker et al. (2009) test different retrievals based on vertical velocity variance,





AMTD
7, 4275–4319, 2014



horizontal wind shear and lidar backscatter from a ship based Doppler lidar during a 44 day campaign in the Gulf of Mexico. A comparison of 99 selected MLHs derived from vertical wind speed and radiosondes gives a correlation of 0.87. During a 10 weeks campaign in a tropical rainforest Pearson et al. (2010) find significantly lower MLH derived from aerosol backscatter than those retrieved from wind lidar, which they attribute to aerosol particle growth within humid layers, gradients in the residual layer, and clouds. A one month campaign in London, Great Britain, described by Barlow et al. (2011) shows good agreement between aerosol and vertical wind based MLH during night but reveals a systematic underestimation of the aerosol based MLH during daytime. Träumner et al. (2011) investigate 12 days of data from different campaigns in Central Europe. A Doppler wind lidar is used to derive MLH from aerosol backscatter and vertical wind speed. Comparison of both retrievals shows a high correlation ($R = 0.91$) but also large scatter with individual differences in the order of 500 m, which are attributed to the fact that the turbulence based height gives the current extent of the ML whereas the aerosol based height gives a measure of past MLH.

The aim of this work is to estimate and compare MLH derived from ceilometer aerosol particle backscatter profiles and from Doppler lidar vertical velocity standard deviation profiles based on one year of continuous observations. The vertical wind speed based MLH retrieval may be seen as a reference as it is based on the variable that causes the vertical mixing, whereas aerosol based retrievals use the aerosol backscatter as a proxy. In this way, the potential performance of a low cost ceilometer network for MLH estimation can be assessed.

## 2 Instruments and retrievals

The following analysis is based on observations by a Vaisala CT25K lidar ceilometer and a HALO Photonics Doppler lidar operated continuously at the Juelich ObservatorY for Cloud Evolution (JOYCE, http://gop.meteo.uni-koeln.de/ag_crewell/doku.php?id=sites:joyce) in Germany at 50°54′ N, 6°24′ E and 111 m a.m.s.l. (above mean sea





AMTD
7, 4275–4319, 2014



level). The CT25K is available since the 1990s and can be considered as a typical low cost network instrument. In order to test its performance with respect to the next generation of ceilometers, we perform an intercomparison with the Jenoptik CMH15K ceilometer over three months. The ceilometers are located within 4 m from each other, and the Doppler lidar is ca. 20 m apart. The instruments and the respective algorithms, i.e. STRAT-2D, to derive MLH are described below. For simplicity the retrieved mixing layer heights are denoted as $MLH_{aero}$ and $MLH_{wind}$ for the aerosol based algorithm and the vertical wind based mixing layer heights, respectively.

## 2.1 Ceilometer

### 2.1.1 Vaisala CT25K

The Vaisala CT25K ceilometer (e.g. Vaisala, 1999; Münkel et al., 2007) collects backscatter data with 15 s temporal and 30 m spatial resolution up to a height of 7.5 km. It operates at 905 nm wavelength, and thus, receives backscatter from cloud droplets and aerosol particles. The average emitted laser pulse energy is 1.6 µJ and 65 536 pulses are averaged to one backscatter profile in order to increase the signal to noise ratio. For further details of the instrument see Table 1. The instrument software provides profiles of the attenuated backscatter coefficient or for short backscatter profiles ($\beta$) which are subsequently input to STRAT-2D. For the CT25K ceilometer, the first range gate starts at 0 m, because a full overlap is achieved by using the same telescope for transmitting and receiving (Münkel et al., 2007).

### 2.1.2 Jenoptik CHM15k

The CHM15k-Nimbus manufactured by Jenoptik GmbH, Germany, operates at 1064 nm wavelength and provides profiles of backscatter up to 15 km with a temporal and spatial resolution of 15 s and 15 m, respectively. Because the optics of the laser and the receiving telescope are separated, sufficient overlap of both optical systems





AMTD
7, 4275–4319, 2014



is reached only at a height of about 350 m. Average pulse energy (8 µJ) and number of pulses averaged to one profile ($N_P \simeq 105\,650$) are higher than those of the Vaisala ceilometer leading to about 8.5 times more emitted photons (see Table 1 and Appendix A). As range gates are shorter and wavelength is larger, the number of backscattered photons reaching the receiving telescope is only about 4.4 times larger. This feature and the more sensitive receiver unit make the CHM15k a significantly advanced ceilometer compared to the CT25K.

The instrument has been operated since August 2013 at JOYCE and provides range and overlap corrected backscatter in arbitrary units. In contrast to earlier studies (e.g. Heese et al., 2010; Wiegner and Geiß, 2012; Martucci et al., 2010) the latest software version used in this study also comprises a correction for the sensitivity fluctuations of the photo avalanche diode of the receiver. This correction significantly increases the temporal stability of retrieved backscatter profiles.

In order to retrieve attenuated backscatter coefficient profiles $\beta$ in appropriate units (i.e. $\mathrm{Sr}^{-1}\,\mathrm{m}^{-1}$) the provided raw backscatter $\beta_{\mathrm{raw}}$ has to be divided by aperture $A$, range gate length $\Delta r$ and the number of emitted photons $N_{\mathrm{emit}}$ calculated from laser pulse energy and wavelength by use of Planck's relation. With every profile the instrument provides self diagnosed state variables for laser $S_{\mathrm{L}}$, optics $S_{\mathrm{O}}$ and receiver $S_{\mathrm{R}}$ in dimensionless units. They are included as $K = S_{\mathrm{L}} \cdot S_{\mathrm{O}} \cdot S_{\mathrm{R}}$ to yield

$$\beta = \frac{\beta_{\mathrm{raw}}}{A \cdot \Delta r \cdot K \cdot N_{\mathrm{emit}}}. \quad (1)$$

As for the CT25K, this variable is then passed on to STRAT-2D to calculate MLH.

### 2.1.3 Mixing layer height retrieval from ceilometer

From several proposed methods for estimating the MLH based on aerosol backscatter profiles we selected the "Structure of the atmosphere" (STRAT-2D) algorithm (Morille et al., 2007; Haeffelin et al., 2012) which is freely available and thus suited for network applications. As most MLH algorithms from backscatter lidar, this method uses the





AMTD
7, 4275–4319, 2014





vertical aerosol backscatter gradient, whereby strong negative gradients can indicate the MLH. However, in order to guarantee a certain temporal consistency of the MLH detection and thus to exclude unphysical outliers, the 2-D version of this algorithm is based on a two dimensional edge detection method (Canny, 1986). It first calculates a gradient in the time-height domain and then further filters for typical edge properties, i.e. there must be a local maximum in the direction of the gradient and gradient pixels must be larger than a threshold or they must have neighbors larger than this threshold. For details see Haeffelin et al. (2012).

Within the STRAT-2D algorithm the $\beta$ profiles are first smoothed using a Gaussian kernel with widths set to 1.2 range gate length (30 m) and 40 time steps (15 s) corresponding to a moving average over 108 m and 30 min. Signal to noise ratio (SNR) is calculated for each bin and values with SNR < 1.3 are not used in further analysis. STRAT-2D then determines three candidates for MLH: The largest ($MLH_{large}$) and second largest gradient ($MLH_{second}$) and the lowest height gradient ($MLH_{low}$). From these three candidates the most probable one is selected depending on the time of the day: During night-time, i.e. from sunset until three hours after sunrise, the lowest height ($MLH_{low}$) is chosen. During daytime only candidates are considered for which the relative vertical backscatter difference is lower than a threshold of 0.9. This condition avoids the signal decay in clouds to be misinterpreted as MLH. The MLH is then the first height from the list $MLH_{large}$, $MLH_{second}$, $MLH_{low}$. If no candidate is found, the lowest valid range gate is returned as boundary layer height.

### 2.1.4 Ceilometer intercomparison

In order to assess the consistency of MLH retrievals from aerosol lidar, the MLH estimates from the two ceilometers are compared. Backscatter data of both instruments from 16 August to 16 November 2013 was analysed with STRAT-2D. As described above, the backscatter data is smoothed equivalently to a running arithmetic average over 30 min and evaluated every 5 min resulting in 26 691 profiles for each instrument. All data below 350 m was rejected for both instruments as the CHM15k suffers from





AMTD
7, 4275–4319, 2014



incomplete overlap up this height. This reduces the number of samples mainly during night-time.

The overall agreement is very good with a bias of 3.6 m. Figure 1 shows the relative difference between MLH from the Vaisala CT25K and the Jenoptik CHM15k over the course of the day. MLH is mainly detected between 08:00 and 18:00 UTC and the median relative difference closely follows the zero line over this period. For a fixed time of day the relative differences are – albeit symmetrically – not following a Gaussian distribution. Therefore instead of a standard deviation we consider the 25 and 75 % percentile for the description of the uncertainty in the derived aerosol mixing layer height $MLH_{aero}$. Over the course of the day these percentiles are relatively constant and correspond to a relative accuracy of ±5 % (Fig. 1).

### 2.2 Wind lidar

Vertical wind speed is measured with a HALO Photonics Streamline wind lidar (Pearson and Collier, 1999; Pearson et al., 2010; Newsom, 2012). It is a coherent Doppler lidar that uses heterodyne detection to measure the Doppler shift of backscattered light. The instrument is based on a near infrared lidar system operating at a wavelength of 1.5 µm. The average pulse energy of 100 µJ is larger than the one of the aerosol lidars used in this study as the Doppler retrieval needs more photons to yield reliable results. Laser pulses are emitted at a frequency of 15 kHz and averaged every second. Processing of these data takes some time resulting in a temporal resolution of 1.67 s. In its current setup, the maximum range is 8 km but the actual range is limited to areas with sufficient occurrence of aerosol. The spatial resolution along the beam is set to 30 m. Largest and smallest resolvable speed are 19.2 and 0.038 $ms^{-1}$, respectively. The output consists of wind speed along the beam, backscatter coefficient and SNR from the heterodyne detection. The instrument is equipped with a scanner to point its beam in any direction of the upper hemisphere. In its current setup, it performs several different scan patterns to infer profiles of horizontal wind speed and its spatial distribution.





AMTD
7, 4275–4319, 2014



These scans sum up to 12 min per hour. During the remaining 48 min per hour the wind lidar points vertically and measures profiles of vertical velocity.

Unreliable Doppler velocities are filtered by a SNR threshold of $SNR_{ts} = -18.2$ dB derived from long-term noise characteristics. This value is somewhat larger than the threshold of −20 dB used by Barlow et al. (2011) based on the considerations of Rye and Hardesty (1993). For the instrument used in this study, the value $SNR_{ts}$ indicates the SNR range below which the Doppler velocity consists only of white noise. It depends on the setup of the instrument, mainly the number of averages, and it differs from instrument to instrument but is constant in space and time.

From the filtered time series of the vertical velocity, the standard deviation $\sigma_w$ is calculated every 5 min over an interval of 30 min. This standard deviation is corrected for instrumental noise following the technique described by Lenschow et al. (2000). Most of the time the correction is less than a few $cms^{-1}$ or a few percent of $\sigma_w$. The average interval of 30 min is motivated by the consideration that a convective plume with an average ascent speed of $1\,ms^{-1}$ needs about 16 min to travel through a mixed layer of 1 km height. The average interval is thus about twice the life time of such a plume and also typical for the derivation of turbulent fluxes from eddy covariance stations.

As shown by Taylor (1922, 1935) the vertical size of a plume growing due to homogeneous turbulent movement is proportional to $\sigma_w$. We thus use $\sigma_w$ as an indicator for vertical mixing. The MLH is determined as the first height where $\sigma_w$ falls below a threshold $\sigma_{wts}$. Different thresholds have been used by Tucker et al. (2009) ($\sigma_{wts} = 0.20$ and $0.17\,ms^{-1}$), Pearson et al. (2010) ($0.30\,ms^{-1}$), Barlow et al. (2011) ($0.32\,ms^{-1}$) and Träumner et al. (2011) ($0.40\,ms^{-1}$). In order to derive a sensible $\sigma_{wts}$ we make use of the semi-theoretical profile of Lenschow et al. (1980) assuming a typical convective velocity scale of $w_\star = 1.5\,ms^{-1}$ and arrive at $\sigma_{wts} = 0.4\,ms^{-1}$ (see Appendix B and Träumner, 2010). However, in reality $w_\star$ is time dependent and the Lenschow et al. (1980) profile is only valid for a developed convective boundary layer. The choice of a threshold





AMTD
7, 4275–4319, 2014



method is of course somewhat unsatisfactory as it makes the retrieval dependent on this value. Such effects are investigated below.

### Threshold sensitivity

To investigate the sensitivity of the MLH derived from Doppler lidar to the threshold in $\sigma_{wts}$ a three month period from June to August 2013 was selected and $\sigma_{wts}$ increased and decreased by 25 % to 0.5 and 0.3 $ms^{-1}$, respectively. Times when the whole $\sigma_w$ profile remained below the threshold were excluded that mainly concerned night-time data. The histogram (Fig. 2) for the relative MLH-changes due the increase/decrease of $\sigma_{wts}$ shows a strong cluster at zero, i.e. in these cases the value of the threshold does not play a role. Nevertheless, the medians are non-zero and absolute differences in MLH average to ±100 m with a linear increase during the day from ±50 m (07:00 UTC) to ±150 m (16:00 UTC) (not shown).

Figure 2 reveals that best agreement occurs between 10:00 and 15:00 UTC, i.e. the time frame in which a well developed boundary layer is most likely. Here, the median of the relative differences caused by a 25 % change in $\sigma_{wts}$ is quite low and accounts to roughly 7 %. It should be noted that both medians are symmetrically to zero indicating that the average $\sigma_w$ shows a linear decrease in this region of the ML. Before 10:00 and after 15:00 UTC the relative differences are higher and we therefore consider ±15 % as error estimate for $MLH_{wind}$. Interestingly, these measurements bring forth similar results as when using the Lenschow et al. (1980) profile that relates a change of $\sigma_w$ by ±25 % to a change in height of ±7 % (see Appendix B). In the morning and afternoon hours the relative difference goes up to ±30 %. This indicates that the Lenschow et al. (1980) profile is only valid around noon in the fully developed ML. In the morning and afternoon hours, the real $\sigma_w$ profile shows a slower decrease with height and consequently the derived MLH depends stronger on the choice of the threshold.





AMTD
7, 4275–4319, 2014



## 3 Results

In this section we first compare the performance of MLH retrievals derived from backscatter and vertical velocity profiles by means of a case study (Sect. 3.1) to illustrate the principle differences between both methods. We then proceed to a statistical analysis (Sects. 3.2–3.3) that distinguishes between all and low cloud cover conditions.

### 3.1 Case study

To investigate the performance of the aerosol based STRAT-2D compared to the wind based MLH retrieval, a fair weather spring day (JOYCE, 28 May 2012) with a classical "textbook" boundary layer development is analyzed (Fig. 3). Between midnight and 08:00 UTC the residual layer is visible as a region with low values of the standard deviation of vertical velocity ($\sigma_w < 0.20\,\mathrm{ms}^{-1}$) up to approx. 1.5 km. Convection begins to develop around 06:00 UTC, i.e. 2.5 h after sunrise, as indicated by enhanced $\sigma_w$ close to the surface. The MLH steadily increases and reaches the maximum RL height at around 09:00 UTC. At 14:00 UTC the ML reaches its maximum height at about 2.1 km and begins to stagnate. Additionally, starting from 10:30 UTC, cumulus clouds start to develop at the top of the ML visible by the high backscatter and subsequent extinction of the signal above in Fig. 3b. Turbulent mixing begins to decay at 16:00 UTC and collapses almost completely throughout the whole ML at 17:30 UTC, two hours before sunset.

Most of the time, both MLH retrievals show good agreement. However, some features revealing typical problems of deriving MLH from backscatter profiles can also be observed (refer to arrows with letters in Fig. 3a). In situation A, the height of the nocturnal boundary layer is interpreted as MLH, although $\sigma_w$ values are well below $0.1\,\mathrm{ms}^{-1}$. Around 07:00 UTC (situation B), aerosol layers within the RL or at its top around 700 m are erroneously retrieved as MLH, although significant mixing is only taking place below 300 m. Finally in situation C (afternoon, starting at 17:00 UTC), the detection of the breakdown of the ML is delayed due to remaining aerosol particles aloft.





AMTD
7, 4275–4319, 2014



In order to gain further insight into the differences between the aerosol and wind based MLH retrievals, the thermal structure of the ABL is considered. Potential temperature profiles are derived from the microwave radiometer HATPRO (Rose et al., 2005). The instrument uses measurements at six different elevation angles to retrieve the vertical profile in the lowest hundred meters of the ABL very accurately with a high resolution of decameters (Löhnert and Meier, 2012). Higher up in the ABL, spatial resolution decreases rapidly, such that the inversion at the top of the boundary layer is usually not resolved.

Potential temperature during night clearly shows the stably stratified and cold nocturnal boundary layer (NBL) with temperatures down to 289 K (04:30 UTC) and gradients of more than +4 K/100 m (01:00–03:00 UTC) close to the surface. The region with pronounced stable stratification grows until 06:00 UTC in the morning (2.5 h after sunrise) when stratification close to the surface quickly transforms from stable to unstable.

During the time span of the lowest temperatures close to the surface, $MLH_{aero}$ increases from 120 m at 03:00 UTC to around 300 m at 04:30 UTC. However, vertical mixing is very unlikely, as stratification at this time is stable with a strong positive potential temperature gradient. In agreement with this, the Doppler lidar did not detect any significant vertical air movement and thus no MLH was assigned (arrow A in Fig. 3a). However, $\beta$ profiles show a region with a significant vertical gradient leading to the detection of a deepening ML between 03:00 and 05:00 UTC. Most probably this development was connected to the dissipation of thin mid-level liquid water clouds (base > 2.5 km, top < 3.2 km as derived from the cloud radar at JOYCE) at 03:00 UTC followed by increased radiative cooling, decreasing temperature (Fig. 4) and increasing relative humidity in the lowest few 100 m. This may have initiated hydrophilic aerosol growth in the stable NBL and consequently an increasing gradient in the backscatter profiles was interpreted as MLH.

Beginning at 06:00 UTC the ML grew into the NBL, dissolved it and further grew in the neutrally stratified RL. Between 07:00 and 08:00 UTC the aerosol derived MLH shows higher values (700 m) than the wind derived MLH (250 m, arrow B in Figs. 3





AMTD
7, 4275–4319, 2014



and 4). Stratification in this region was still stable and vertical wind as low as during the night. Aerosol backscatter below the wind derived MLH showed enhanced values, nevertheless, the gradient in $\beta$ at this height seems to be lower than gradients in the RL above or even at the top of the RL and these heights are consequently assigned as MLH. The most probable explanation for this behaviour is that with the breakup of the NBL temperature increases, relative humidity decreases and backscatter decreases as well. The backscatter gradient at the top of the ML becomes smaller than gradients in the RL above.

The third situation (arrow C in Figs. 3 and 4) illustrates that the aerosol based STRAT-2D algorithm cannot follow the breakdown of the MLH around 17:45 UTC. Instead, the top of the aerosol layer, which at this time is the top of the RL, is identified as the MLH. Unfortunately, it is not possible to analyze the temperature inversion at the top of the ABL due to low spatial resolution of the MWR data at these heights. However, Träumner et al. (2011) already noted that incorrect detection during MLH decay is due to the fact that the aerosol distribution in the ABL represents the history of the mixing processes, whereas the vertical wind shows the current status of vertical mixing.

### 3.2 Average diurnal cycle

After discussing typical issues concerning MLH detection from aerosol backscatter profiles in comparison to the more realistic retrievals from wind lidar in the section above, we now analyze the impacts of the different retrievals on the average diurnal cycle of the MLH. The analysis is carried out over the course of one full year (4 seasons) of JOYCE observations between December 2011 and November 2012 (Fig. 5). Values below 120 m are excluded as both retrievals fall back to values below if no MLH could be found which was the case for about 50 % of the data. Time series are synchronized and values are only accepted when both retrievals provide a value. When less than 20 % of the original data remains, statistics are not evaluated which mainly excludes the night time values. Note, that the analysis is carried out for all cases including cloudy (e.g. frontal passages and cumulus clouds) and clear sky cases.





AMTD
7, 4275–4319, 2014



### 3.2.1 All cases

The MLH from both methods shows an increase in the morning until noon in spring and summer (MAM and JJA in Fig. 5) which is in general agreement with the common knowledge of the development of a convective boundary layer (e.g. Stull, 1988). During spring (summer) the average $MLH_{wind}$, begins to decrease two (three) hours before sunset. In contrast to this, $MLH_{aero}$ remains longer at higher MLH values, decreasing in height with sunset (spring, MAM) or two hours before the earliest sunset (summer, JJA). This behavior generalizes the difference between $MLH_{wind}$ and $MLH_{aero}$ already noted in situation within the case study (Figs. 3 and 4). In the morning hours before noon, average $MLH_{aero}$ is in general larger and shows a smaller growth rate than $MLH_{wind}$. This could be related to situations denoted as B in the case study above (Figs. 3 and 4). In contrast to the other seasons, night-time values above the minimum ML are frequently retrieved by both methods in winter (DJF). The switch of the STRAT-2D algorithm between the day mode (beginning 3 h after sunrise) and the night mode (beginning with sunset) is clearly visible. As Fig. 5 shows, the aerosol based MLH retrieval during daytime is generally 400 m higher than night-time, while the vertical velocity driven $MLH_{wind}$ shows no diurnal cycle.

The variability of MLH as depicted by the difference between the 25 and 75 % percentiles is around 500 m in all seasons (except winter) and most times of day (Fig. 5). In winter the STRAT-2D algorithm provides a nearly constant MLH of about 400 m during night-time with very little variability.

In general, the difference $\Delta MLH = MLH_{aero} - MLH_{wind}$ is positive for all seasons except for night-time in winter (Fig. 6). This could be expected as the wind retrieval of a Doppler wind lidar depends on aerosol backscatter. They should be equal in case of a fully developed ML above which only clean air of the free troposphere and thus no backscatter can be found. In the case of a developing ML, which grows into the RL, there might be aerosol above and $MLH_{aero}$ could be larger than $MLH_{wind}$. In contrast the comparison by Pearson et al. (2010) showed $MLH_{wind}$ to be larger than $MLH_{aero}$





AMTD
7, 4275–4319, 2014



but as their measurements were taken in the tropics, humidity might have affected the aerosol particle properties. Träumner (2010) mentions that in individual cases $MLH_{wind} > MLH_{aero}$ could be observed. From our study it is obvious that on average $MLH_{wind} \leq MLH_{aero}$ holds.

The spread of the differences between both MLHs, depicted by the difference between the 25 and 75 % percentiles, is rather large with values up to 500 m (Fig. 6) but in the same order of magnitude as the 600 m reported by Haeffelin et al. (2012) for differences between an aerosol based retrieval and radiosondes. The spread is largest in the afternoon and larger in summer than in spring and autumn. Considering the error estimate based on the sensitivity studies in Sects. 2.1.4 and Sect. "Threshold sensitivity" the differences are significant most of the time, particularly in the late afternoon in spring, summer and autumn (Fig. 6).

In spring, summer and autumn, mean and median of ΔMLH show the same behaviour: larger differences in the morning and afternoon hours and values closer to zero around noon. The overestimation of $MLH_{aero}$ is strongest in the morning and the late afternoon during these seasons. The largest differences occur in the late afternoon reaching average and median values of 600 m which is in the order of the MLH itself at that time of the day. Similarly, in the morning, the difference in MLH is of the order of 300 m. This pattern of MLH differences does not appear during winter (DJF) when convective conditions are rather rare. Therefore, the observed differences were dominated by synoptic forcing with no preference for any time of the day in winter.

Because spring, summer and autumn statistics also include many different weather situations, the retrievals might be biased by other atmospheric phenomena such as precipitation, layers within stable stratification or clouds. As the classical definition of MLH development mostly applies during fair weather conditions, the following analysis is restricted to cases where cloud cover is low. A threshold of 4 octa for clouds with base height lower than 3 km is arbitrarily chosen. The amount of cloud cover was determined from the ceilometer data as the relative occurrence of cloud base height below 3 km during a period of 30 min.





AMTD
7, 4275–4319, 2014



### 3.2.2 Cloudy cases excluded

By excluding cloudy situations the total number of cases is further reduced by about 45 % (summer and spring), 50 % (autumn) and 70 % (winter) and leads to the removal of the night-time values also in winter as not enough cases for a statistical evaluation remain. Retrieved MLHs become slightly higher in all seasons (Fig. 7). When comparing MLHs from the two methods, one can see that the qualitative differences in temporal evolution remain similar to the results shown in Fig. 5. However, a quantitative comparison makes clear that the differences in MLH are now even larger by about 100 m in the morning and in the evening during spring, summer and autumn (Fig. 7). Again, close to zero differences in the MLH before and at noon were observed in spring and summer. It should also be noted that the number of cases with $MLH_{aero} < MLH_{wind}$ are reduced. In winter, a pattern with high differences in the morning and evening hours and a minimum in the early afternoon can be observed. This pattern is similar to the summer and spring cases and it is likely, that this is a typical feature of convective boundary layers.

## 3.3 Statistical analysis

A way of more clearly visualizing the differences between the two MLH retrievals are joint histograms of $MLH_{wind}$ and $MLH_{aero}$. These have been calculated as a function of season, once for all cases (Fig. 8) and once for low-cloud-cover cases (Fig. 9). Statistical measures describing the relation of both data sets are given in Table 2.

When regarding the all-sky cases (Fig. 8), a clustering along the main diagonal can be observed in spring, summer and autumn. In addition, another area of frequent occurrence can be identified where $MLH_{aero}$ values are above or around 1 km while $MLH_{wind}$ is much lower. In order to explain this feature the temporal evolution of the half hourly averaged MLHs during the course of day from Fig. 5 is included in Fig. 8. Especially in spring and summer a hysteresis effect is visible: $MLH_{aero}$ starts in the morning with values larger than $MLH_{wind}$ and reaches the values of $MLH_{wind}$ around noon but remains in the afternoon at high levels whereas $MLH_{wind}$ is already





AMTD
7, 4275–4319, 2014



decreasing. The average $MLH_{aero}$ values higher than 1.2 km, that are not matched by their $MLH_{wind}$ counterparts, occur after noon and are related to the fact, that aerosol backscatter based MLHs remain at higher altitudes until sunset (see Sect. 3.1 and point C in Fig. 3). Also visible but less pronounced is a systematic overestimation of MLH from the aerosol profiles before noon. This can be related to the difficulty in finding the boundary between the deepening ML and the RL above in the backscatter profiles (see Sect. 3.1 and point B in Fig. 3).

The frequent occurrence of $MLH_{aero} > MLH_{wind}$ in spring, summer and autumn leads to low slopes ($\leq 0.46$), large offsets ($\geq 590$ m) and low correlation coefficients ($R \leq 0.43$) for the linear fit (Table 2). Especially in winter many cases are present with $MLH_{wind} > MLH_{aero}$ which mostly occur during night when the STRAT-2D algorithm is in night mode and prefers the lowest MLH candidate. Accordingly, the bias is only negative in winter, and correlation coefficient and slope are the lowest for the all-data sample.

Excluding the cloudy cases decreases the number of cases with shallow MLH below 500 m in spring and summer and thus increases the relative contribution of cases with larger MLHs (Fig. 9). As a result, the offsets of the linear fit increase (Table 2). Similarly the relative contribution of cases with $MLH_{aero} > MLH_{wind}$ increases which especially in spring leads to a decrease of slope and correlation coefficient whereas in summer both remain more or less the same. The bias increases in both seasons which is a direct result of the larger differences we already saw in Sect. 3.2. In winter, the main effect of omitting cloudy data is the removal of night-time values with small MLH and especially $MLH_{aero} < MLH_{wind}$. Cases with $MLH_{aero} > MLH_{wind}$ gain now much more weight in the statistics. This increases slope and offset of the linear fit, reduces the regression coefficient and makes the bias positive. Autumn is somehow opposite: the relative contribution of low MLH close to the main diagonal increases and thus slope and regression coefficient increase. But as the relative contribution of off-diagonal elements increase, the bias increases as well. Summarizing these results, it can be said that





AMTD
7, 4275–4319, 2014



excluding cloudy cases increases the contribution of cases with $MLH_{aero} > MLH_{wind}$ in all seasons which accordingly must be a feature of convective boundary layers.

### 3.4 Connection of MLH to clouds

Cumulus clouds are directly connected to the atmospheric boundary layer as they are the convective plumes which become visible due to condensation. Figure 10 shows a 2-D histogram of cloud base heights (CBH) with the average MLHs from aerosol and wind based retrieval overlayed. Cloud bases are those reported every 15 s by the Vaisala ceilometer. The cloud base statistic is similar to what Brümmer et al. (2012) found in a 7 year statistic from a site near Hamburg about 380 km to the northeast from JOYCE under similar climatic conditions (Fig. 18 in Brümmer et al., 2012). A similar pattern can also be found in the Climate Modeling Best Estimate data set (CMBE, Fig. 3a in Xie et al., 2010).

In the presented study we can show that in spring and summer CBHs are frequently at the same height as the average MLH. They follow the diurnal course of the MLH from the morning until afternoon. In autumn and winter this distinct connection between MLH and CBH is not visible. Instead, in autumn there is a cluster around 1 km which might be related to dissolving stratus clouds. In Winter highest frequencies for cloud bases are in the lowest few hundred meters which is related to fog.

The strong connection between MLH and CBH in spring and summer coincides with the general experience that the base of cumulus clouds is located always more or less at the top of the boundary layer but never significantly below and of course never above (see e.g. studies on shallow tradewind cumulus Riehl et al., 1951; Augstein et al., 1974). The mechanism can be described as follows: the ML grows until it reaches the cumulus condensation level (CCL) and cumulus clouds form. Incident solar radiation at the surface is reduced, convection becomes weaker and ML growth is reduced. Warming and drying of the ML lifts the CCL and cloud cover is reduced. Incident solar radiation and thus convection increases and again influences the cloud cover. Several studies used Large eddy simulation (LES) to understand the role of the different fluxes





AMTD
7, 4275–4319, 2014



in the mass and heat budget of the cumulus topped BL (see e.g. Brown et al., 2002). Others investigate mass flux schemes suitable for climate models (e.g. Neggers et al., 2004). All these models show that there is a strong coupling between LCL and MLH.

As the determination of cloud base height is simpler than the determination of mixed layer height it could be used as a good proxy for MLH at least during convective situations.

## 4 Summary and conclusions

We analysed and compared one year of mixed layer heights (MLH) derived from (i) aerosol backscatter and (ii) standard deviation of the vertical wind speed. For (i) we used backscatter data from a Vaisala CT25K ceilometer and the STRAT-2D algorithm with its core based on an edge detection algorithm (Sect. 2.1). For (ii) we used vertical wind speed data from a HALO Photonics streamline wind lidar and a threshold algorithm (Sect. 2.2). The basic idea is that the vertical velocity is a direct measure for the turbulent mixing while in contrast hereto the backscatter profile is only a proxy for the mixing process. Although there is some uncertainty about how to exactly determine MLH from vertical wind (Sect. “Threshold sensitivity”), the retrieved wind based MLH with a relative error estimated to be 15 % can serve as a reference. In contrast to former studies which mostly concentrate on case studies we present here a one year, four season climatology and a quantitative comparison between the two methods.

In general, MLH from both methods follows the typical evolution of a convectively growing mixed layer. However, the method based on aerosol backscatter profiles typically overestimates the MLH throughout the day, and especially can not follow the mixed layer evolution in the morning and late afternoon hours (Sect. 3.2). The MLH differences between the methods are on their lowest (in the order of 100 m) around noon and had distinct maxima in the morning when the ML grows into the RL and in the late afternoon when turbulence decays. These differences become larger when cloudy





AMTD
7, 4275–4319, 2014



cases are excluded from the analysis indicating that these differences are connected to convective conditions.

Table 3 summarises the performance of the two methods on days with convection and low cloud cover or clear sky conditions. Our analysis indicates that retrieving MLH with the backscatter based method is more challenging than with the vertical velocity based method for the following reasons.

Although the single year of measurements did not provide enough values during night we could show in a case study that during night when there is no vertical wind the aerosol based method can be mislead by alternating layers of high and low aerosol backscatter (cf. Sect. 3.1 and situation A in Fig. 3). These layers can be caused by advection of layers of e.g. aerosol rich air in the residual layer (RL) but also by enhanced backscatter due to high relative humidity in the NBL close to the surface. In the same manner, the boundary between the aerosol rich RL and the clear free troposphere above could be misinterpreted as MLH. The STRAT-2D algorithm tries to avoid these false attributions by using between sunset and three hours after sunrise a night-time mode which prefers the lowest detected significant backscatter gradient. However, this switch is rather crude and cannot really avoid the detection of aerosol layers as MLs.

A mixing layer height retrieval based on vertical wind during night seems to be simple: in the stably stratified NBL vertical movement is suppressed and vertical velocities are close to zero. Strong wind shear due to e.g. the nocturnal low level jet (NLLJ) may lead to intermittent turbulence which is an occasional and locally constricted event (Van de Wiel et al., 2003). These events can cause effective mixing between layers, but might be missed with a vertically pointing instrument which can see only events at its own location. This might be overcome by using scanning measurements (Banta et al., 2006, e.g.). Furthermore, mixing may occur only in a shallow layer close to the ground and thus below the overlap region of the Doppler lidar. Synergetic deployment of Doppler lidar and sodar (Sound Detection and Ranging) would also improve detection of shallow nocturnal mixed layers (Wood et al., 2013).





AMTD
7, 4275–4319, 2014



Before noon, when the ML grows into the RL, no clear backscatter gradient between the two layers is frequently present (situation B in Fig. 3). In such cases, the aerosol based retrieval finds either the top of the aerosol layer, which coincides with the top of the RL, or remaining aerosol layers within the RL. In contrast hereto the vertical wind allows a clear discrimination between the ML and RL. These events occur frequently as confirmed by an average overestimation of $MLH_{aero}$ of up to 400 m in spring, summer and autumn (Figs. 6 and 7).

Around noon when the mixed layer is fully developed, its top is also the top of the aerosol layer with no backscatter gradient below and accordingly a non-ambiguous aerosol based MLH retrieval. As a Doppler wind lidar depends on sufficient backscatter it will tend to report the same height that is underlined by the observed minimum in ΔMLH around noon in our long-term assessment.

In the late afternoon when turbulence decays, aerosol particles still remain well mixed and no clearly detectable gradient at the top of the descending mixed layer can be identified. Instead, any aerosol based algorithm will continue to identify the top of the aerosol layer as MLH which at this time of the day is already the top of the RL. Similar observations have also been made by other studies (e.g Träumner et al., 2011; Baars et al., 2008). But one has to consider that at that time of the day MLH retrieval based on the vertical wind has also its shortcomings: the decay of the convective turbulence is a transition to a more intermittent regime, i.e. plumes which reach the top of the ML become less frequent. As a result $\sigma_w$ decays only gradually with time and the exact moment when the retrieval reports the break down of convective mixing depends strongly on the threshold. The standard deviation of vertical wind speed may also fluctuate in time and the retrieved MLH may jump between low and high values if the fluctuation is around the threshold. We also observed late afternoon cases when active plumes were advected in the upper two thirds of the BL only, while the lower third was calm. The retrieval then reported no MLH as no mixing between the surface and the layers above occured. However, these cases are rare and in general the decay of turbulence occurs similarly at all levels. The long-term assessment shows average





AMTD
7, 4275–4319, 2014



differences between aerosol and wind based MLH reaching up to 800 m around one hour before sunset (Figs. 6 and 7).

As described by White et al. (2009) state of the art dispersion models could be significantly improved by providing measured mixing layer height as input. Ceilometers are widespread, e.g. at airports, and can provide continuous MLH estimates in networks (Haeffelin et al., 2012). We could show that aerosol based MLH estimates suffer from systematical overestimation in the order of several 100 m, especially in the morning and late afternoon hours when emissions from individual traffic are largest. Concentrations of surface emitted pollutants in the mixed layer scale directly with the height of the ML. Accordingly, this overestimation would significantly alter predictions of concentrations towards too low values.

## Appendix A

### Compare ceilometers

The key parameters to describe a lidar are wavelength $\lambda$, energy per pulse $E_0$, number of pulses averaged to one profile $N_P$, opening area of the receiving telescope (aperture $A$), range gate length ($\Delta r$) and beam diameter ($D$). The receiver is usually an avalanche photodiode (APD, the semiconductor equivalent to a photomultiplier) which in principle counts single photons. Thus the number of typically send and received photons is a good measure to compare two instruments.

The number of emitted photons $N_0$ is the energy per pulse $E_P$ divided by the energy per photon $E_0$ which depends on wavelength $\lambda$ (Plancks relation). It is $E_0 = h \cdot c/\lambda$ with Plancks constant $h$ and speed of light $c$, and thus $N_0 = E_P \cdot \lambda/(h \cdot c)$. For the average profile, $N_m = N_0 \cdot N_P$ photons are emitted. Comparing two instruments $A$ and $B$ the relation between the emitted photons is

$$\frac{N_{mA}}{N_{mB}} = \frac{E_{PA} \cdot \lambda_A \cdot N_{PA}}{E_{PB} \cdot \lambda_B \cdot N_{PB}}. \quad \text{(A1)}$$





AMTD
7, 4275–4319, 2014



The number of back scattered photons $N_\beta$ depends on the wavelength and the type of aerosol. The wavelength dependence can be estimated by a power law: $N_\beta \sim \lambda^{-\nu_{\text{mie}}}$ with Angstrom exponent $\nu_{\text{mie}}$ which is for continental aerosol typically of the order of 1 ... 1.8. The number also depends on the number of scattering particles and thus on size of the volume i.e. range gate length $\Delta r$ and square of the beam diameter $D$, i.e. $N_\beta \sim \Delta r \cdot D^2$. Finally only those photons which reach the telescope have a chance to be counted by the APD, thus it must be proportional to the aperture ($A$). We thus get for the received photons $N_\text{r}$:

$$\frac{N_{\text{rA}}}{N_{\text{rB}}} = \frac{E_{\text{PA}} \cdot \lambda_{\text{A}}^{1-\nu_{\text{mie}}} \cdot N_{\text{PA}} \cdot \Delta r_{\text{A}} \cdot D_{\text{A}}^2}{E_{\text{PB}} \cdot \lambda_{\text{B}}^{1-\nu_{\text{mie}}} \cdot N_{\text{PB}} \cdot \Delta r_{\text{B}} \cdot D_{\text{B}}^2}. \tag{A2}$$

Of course this estimate does not take into account the furhter pathway within the instrument, i.e. transmittance of the optics, bandwidth of the filters, sensitivity and dynamic range of the receiver, etc.

We operate two ceilometers at JOYCE: a Vaisala CT25K and a Jenoptik CHM15k with parameters depicted in Table 1. Although the Jenoptik emits nearly ten times more photons the number of potentially received photons per range gate is only 4.4 times larger than for the Vaisala. The main loss is due to the shorter range gate length. As the Jenoptik shows in general a much better sensitivity and less noise it can be concluded that the receiver is better.

## Appendix B

## The Lenschow profile

Lenschow et al. (1980) derived a universal profile for $\sigma_w$ based on a handful of airplane measurements and scaling considerations. Scaling parameter for height should be the height of the mixing laxer $h$. Velocity should scale with the convective velocity scale





AMTD
7, 4275–4319, 2014



proposed by Deardorff (1970). Close to the surface the height dependence should be of the form $(z/h)^{1/3}$, at the surface $\sigma_w$ should be zero and the profile should have a maximum in the lower half of the mixing layer. He proposed the following form:

$$\sigma_w = w_\star \cdot c_1 \cdot \zeta^\nu \cdot (1 - c_2 \cdot \zeta)^\mu \tag{B1}$$

with $\zeta = z/h$ the height scaled with mixing layer height $h$ and parameters $c_1 = \sqrt{1.8} = 1.34$, $c_2 = 0.8$, $\nu = \frac{1}{3}$ and $\mu = 1$. At the top of the ML, at $\zeta = 1$, the profile does not become zero, it is:

$$\sigma_w(\zeta = 1) = w_\star \cdot c_1 \cdot (1 - c_2)^\mu = 0.268 \cdot w_\star. \tag{B2}$$

The derivative with respect to $\zeta$ is

$$\frac{\partial \sigma_w}{\partial \zeta} = \sigma_w \cdot \left( \frac{\nu}{\zeta} - \frac{c_2}{1 - c_2 \zeta} \right). \tag{B3}$$

At the maximum the derivative is zero, leading to

$$\zeta_{\max} = \frac{\nu}{c_2 \cdot (\mu + \nu)} = 0.312. \tag{B4}$$

The value $\sigma_{w\max}$ at this height is

$$\sigma_{w\max} = w_\star \cdot c_1 \cdot \zeta_{\max}^\nu \cdot (1 - c_2)^\mu = 0.682 \cdot w_\star. \tag{B5}$$

The value at ML top can be expressed relative to the value of the maximum:

$$\sigma_w(\zeta = 1) = 0.393 \cdot \sigma_{w\max}. \tag{B6}$$

The profile can also be utilized to estimate the dependence of the MLH estimate from the threshold. Using $\frac{\partial \sigma_w}{\partial \zeta} \frac{1}{\sigma_w} \simeq \frac{\Delta \sigma_w}{\sigma_w} \frac{h}{\Delta z}$ at mixed layer top ($\zeta = 1$) the relative change of determined MLH with a relative change of threshold $\sigma_{\text{wts}}$ becomes

$$\frac{\Delta \text{MLH}}{\text{MLH}} = \frac{1}{\nu - \frac{c_2}{1 - c_2}} \cdot \frac{\Delta \sigma_{\text{wts}}}{\sigma_{\text{wts}}} = -0.273 \cdot \frac{\Delta \sigma_{\text{wts}}}{\sigma_{\text{wts}}}. \tag{B7}$$





AMTD
7, 4275–4319, 2014



That means that with an increase (decrease) of $\sigma_{wts} = 0.4\,ms^{-1}$ by $0.1\,ms^{-1}$ (i.e. 25 %) the detected MLH would decrease (increase) by 7 %.

*Acknowledgements.* We gratefully acknowledge financial support by the SFB/TR 32 "Pattern in Soil-Vegetation-Atmosphere Systems: Monitoring, Modelling, and Data Assimilation" funded by the Deutsche Forschungsgemeinschaft (DFG). Work by A. Hirsikko was supported within the project High Definition Clouds and Precipitation for advancing Climate Prediction HD(CP)$^2$ funded by the German Ministry for Education and Research under grant FK 01LK1209B. We thank Kerstin Ebell for proofreading the manuscript.

## References

American Meteorological Society: Glossary of Meteorology, American Meteorological Society, http://glossary.ametsoc.org/, last access: 25 April 2014. 4276

Augstein, E., Schmidt, H., and Wagner, V.: The vertical structure of the atmospheric planetary boundary layer in undisturbed Trade winds over the Atlantic Ocean, Bound.-Lay. Meteorol., 6, 129–150, doi:10.1007/BF00232480, 1974. 4294

Baars, H., Ansmann, A., Engelmann, R., and Althausen, D.: Continuous monitoring of the boundary-layer top with lidar, Atmos. Chem. Phys., 8, 7281–7296, doi:10.5194/acp-8-7281-2008, 2008. 4279, 4297

Banta, R. M., Pichugina, Yelena, L., and Brewerm, W. A.: Turbulent Velocity-Variance Profiles in the Stable Boundary Layer Generated by a Nocturnal Low-Level Jet, J. Atmos. Sci., 63, 2700–2719, doi:10.1175/JAS3776.1, 2006. 4277, 4296

Barlow, J. F., Dunbar, T. M., Nemitz, E. G., Wood, C. R., Gallagher, M. W., Davies, F., O'Connor, E., and Harrison, R. M.: Boundary layer dynamics over London, UK, as observed using Doppler lidar during REPARTEE-II, Atmos. Chem. Phys., 11, 2111–2125, doi:10.5194/acp-11-2111-2011, 2011. 4279, 4280, 4285

Brooks, I.: Finding boundary layer top: application of a wavelet covariance transform to lidar backscatter profiles, J. Atmos. Ocean. Tech., 20, 1092–1105, doi:10.1175/1520-0426(2003)020<1092:FBLTAO>2.0.CO;2, 2003. 4278





AMTD

7, 4275–4319, 2014



Brown, A., Chlond, A., Golaz, C., Khairoutdinov, M., Lewellen, D., Lock, A., MacVean, M., Moeng, C.-H., Neggers, R., Siebesma, A., and Stevens, B.: Large-eddy simulation of the diurnal cycle of shallow cumulus convection over land, Q. J. Roy. Meteorol. Soc., 128, 1075–1094, doi:10.1256/003590002320373210, 2002. 4295

Brümmer, B., Lange, I., and Konow, H.: Atmospheric boundary layer measurements at the 280 m high Hamburg weather mast 1995–2011: mean annual and diurnal cycles, Meteorol. Z., 21/4, 319–335, doi:10.1127/0941-2948/2012/0338, 2012. 4294

Canny, J.: A Computational Approach to Edge Detection, IEEE T. Patt. Anal. Mach. Intell., 8, 679–698, doi:10.1109/TPAMI.1986.4767851, 1986. 4283

Cohn, S. A. and Angevine, W. M.: Boundary Layer Height and Entrainment Zone Thickness Measured by Lidars and Wind-Profiling Radars, J. Appl. Meteorol., 39, 1233–1247, doi:10.1175/1520-0450(2000)039<1233:BLHAEZ>2.0.CO;2, 2000. 4279

Collier, C., Davies, F., Bozier, K., Holt, A., Middleton, D., Pearson, G., Siemen, S., Willetts, D., Upton, G., and Young, R.: Dual-Doppler Lidar Measurements for Improving Dispersion Models, B. Am. Meteorol. Soc., 86, 825–838, doi:10.1175/BAMS-86-6-825, 2005. 4277

Davis, K., Gamage, N., Hagelberg, C., Kiemle, C., Lenschow, D., and Sullivan, P.: An objective method for deriving atmospheric structure from airborne lidar observations, J. Atmos. Ocean. Tech., 17, 1455–1468, doi:10.1175/1520-0426(2000)017<1455:AOMFDA>2.0.CO;2, 2000. 4278

Deardorff, J.: Convective Velocity and Temperature Scales for the Unstable Plantery Boundary Layer and for Rayleigh Convection, J. Atmos. Sci., 27, 1211–1213, doi:10.1175/1520-0469(1970)027<1211:CVATSF>2.0.CO;2, 1970. 4300

Emeis, S., Schäfer, K., and Münkel, C.: Surface-based remote sensing of the mixing-layer height – a review, Meteorol. Z., 17, 621–630, doi:10.1127/0941-2948/2008/0312, 2008. 4278

Endlich, R., Ludwig, F., and Uthe, E.: An automatic method for determining the mixing depth from lidar observations, Atmos. Environ., 13, 1051–1056, doi:10.1016/0004-6981(79)90015-5, 1979. 4278

Eresmaa, N., Karppinen, A., Joffre, S. M., Räsänen, J., and Talvitie, H.: Mixing height determination by ceilometer, Atmos. Chem. Phys., 6, 1485–1493, doi:10.5194/acp-6-1485-2006, 2006. 4278, 4279





AMTD
7, 4275–4319, 2014



Eresmaa, N., Härkönen, J., Joffre, S., Schultz, D., Karppinen, A., and Kukkonen, J.: A Three-Step Method for Estimating the Mixing Height Using Ceilometer Data from the Helsinki Testbed, J. Appl. Meteorol. Clim., 51, 2172–2187, doi:10.1175/JAMC-D-12-058.1, 2012. 4278, 4279

Garratt, J.: The Atmospheric Boundary Layer, Cambridge University Press, Cambridge, England, 1994. 4277

Haeffelin, M., Angelini, F., Morille, Y., Martucci, G., Frey, S., Gobbi, G. P., Lolli, S., O'Dowd, C. D., Sauvage, L., Xueref-Rémy, I., Wastine, B., and Feist, D. G.: Evaluation of Mixing-Height Retrievals from Automatic Profiling Lidars and Ceilometers in View of Future Integrated Networks in Europe, Bound.-Lay. Meteorol., 143, 49–75, doi:10.1007/s10546-011-9643-z, in press, 2012. 4278, 4279, 4282, 4283, 4291, 4298

Haij, M. D., Wauben, W., and Klein Baltink, H.: Determination of mixing layer height from ceilometer backscatter profiles, Proc. SPIE, 6362, 63620R, doi:10.1117/12.691050, 2006. 4278

Haij, M. D., Wauben, W., and Klein Baltink, H.: Continuous mixing layer height determination using the LD-40 ceilometer: a feasibility study, Tech. Rep. KNMI Scientific Report WR 2007-01, KNMI, De Bilt, the Netherlands, 2007. 4278

Heese, B., Flentje, H., Althausen, D., Ansmann, A., and Frey, S.: Ceilometer lidar comparison: backscatter coefficient retrieval and signal-to-noise ratio determination, Atmos. Meas. Tech., 3, 1763–1770, doi:10.5194/amt-3-1763-2010, 2010. 4282

Hogan, R., Grant, A., Illingworth, A., Pearson, G., and O'Connor, E.: Vertical velocity variance and skewness in clear and cloud-topped boundary layers as revealed by Doppler lidar, Q. J. Roy. Meteorol. Soc., 135, 635–643, doi:10.1002/qj.413, 2009. 4279

Lenschow, D. H., Wyngaard, J. C., and Pennell, W. T.: Mean-Field and Second-Moment Budgets in a Baroclinic, Convective Boundary Layer, J. Atmos. Sci., 37, 1313–1326, doi:10.1175/1520-0469(1980)037<1313:MFASMB>2.0.CO;2, 1980. 4279, 4285, 4286, 4299, 4311

Lenschow, D. H., Wulfmeyer, V., and Senff, C.: Measuring second- through fourth-order moments in noisy data, J. Atmos. Ocean. Tech., 17/10, 1330–1347, doi:10.1175/1520-0426(2000)017<1330:MSTFOM>2.0.CO;2, 2000. 4285

Löhnert, U. and Maier, O.: Operational profiling of temperature using ground-based microwave radiometry at Payerne: prospects and challenges, Atmos. Meas. Tech., 5, 1121–1134, doi:10.5194/amt-5-1121-2012, 2012. 4288





AMTD
7, 4275–4319, 2014



Martucci, G., Milroy, C., and O'Dowd, C.: Detection of cloud-base height using Jenoptik CHM15K and Vaisala Cl31 Ceilometers, J. Atmos. Ocean. Tech., 27, 305–318, doi:10.1175/2009JTECHA1326.1, 2010. 4282

Martucci, G., Chauvigne, A., O'Connor, E. J., Hirsikko, A., Ceburnis, D., Wobrock, W., and O'Dowd, C. D.: Ground-based remote sensing profiling of aerosols, boundary layer and liquid water clouds using synergistic retrievals, in: Proceedings of the 9th International Symposium on Tropospheric Profiling, September 2012, L'Aquila, Italy, http://cetemps.aquila.infn.it/istp/proceedings/Session_C_Aerosols_clouds_and_precipitation/Session_C_Tuesday_4_September_2012/SC_05_Martucci.pdf (last access: 25 April 2014), 2012. 4279

Morille, Y., Haeffelin, M., Dobrinski, P., and Pelon, J.: STRAT: An Automated Algorithm to Retrieve the Vertical Structure of the Atmosphere from Single-Channel Lidar Data, J. Atmos. Ocean. Tech., 24, 761–775, doi:10.1175/JTECH2008.1, 2007. 4282

Münkel, C., Eresmaa, N., Räsänen, J., and Karppinen, A.: Retrieval of mixing height and dust concentration with lidar ceilometer, Bound.-Lay. Meteorol., 124, 117–128, doi:10.1007/s10546-006-9103-3, 2007. 4278, 4279, 4281

Neggers, R. A. J., Siebesma, A. P., Lenderink, G., and Holtslag, A. A. M.: An Evaluation of Mass Flux Closures for Diurnal Cycles of Shallow Cumulus, Mon. Weather Rev., 132, 2525–2538, doi:10.1175/MWR2776.1, 2004. 4295

Newsom, R.: Doppler Lidar (DL) Handbook, Tech. Rep. DOE/SC-ARM-TR-101, ARM Climate research facility, http://www.arm.gov/publications/tech_reports/handbooks/dl_handbook.pdf (last access: 25 April 2014), 2012. 4284

O'Connor, E. J., Illingworth, A. J., Brooks, I. M., Westbrook, C. D., Hogan, R. J., Davies, F., and Brooks, Barbara, J.: A Method for Estimating the Turbulent Kinetic Energy Dissipation Rate from a Vertically Pointing Doppler Lidar, and Independent Evaluation from Balloon-Borne In Situ Measurements, J. Atmos. Ocean. Tech., 27, 1652–1664, doi:10.1175/2010JTECHA1455.1, 2010. 4278, 4279

Oke, T.: Boundary Layer Climates, Methuen & Co., London, England, 1987. 4276

Pearson, G. and Collier, G.: A pulsed coherent $CO_2$ lidar for boundary layer meteorology, Q. J. Roy. Meteorol. Soc., 125, 2703–2721, doi:10.1002/qj.49712555918, 1999. 4284

Pearson, G., Davies, F., and Collier, C.: Remote sensing of the tropical rain forest boundary layer using pulsed Doppler lidar, Atmos. Chem. Phys., 10, 5891–5901, doi:10.5194/acp-10-5891-2010, 2010. 4279, 4280, 4284, 4285, 4290





AMTD
7, 4275–4319, 2014



Riehl, H., Yeh, C., Malkus, J., and LaSeur, N.: The northeast trade of the Pacific Ocean, Q. J. Roy. Meteorol. Soc., 77, 598–626, doi:10.1002/qj.49707733405, 1951. 4294

Rose, T., Crewell, S., Löhnert, U., and Simmer, C.: A network suitable microwave radiometer for operational monitoring of the cloudy atmosphere, Atmos. Res., 75, 183–200, doi:10.1016/j.atmosres.2004.12.005, 2005. 4288

Rye, B. J. and Hardesty, R. M.: Discrete spectral peak estimation in incoherent backscatter heterodyne lidar, II: correlogram accumulation, IEEE T. Geosci. Remote, 31, 28–35, doi:10.1109/36.210441, 1993. 4285

Seibert, P., Beyrich, F., Gryning, S.-E., Joffre, S., Rasmussen, A., and Tercier, P.: Review and intercomparison of operational methods for the determination of the mixing height, Atmos. Environ., 34, 1001–1027, doi:10.1016/S1352-2310(99)00349-0, 2000. 4277, 4278

Senff, C., Bösenberg, J., Peters, G., and Schaberl, T.: Ozone Budget in the Convective Boundary Layer with DIAL and Radar-RASS: A Case Study, Contrib. Atmos. Phys., 96, 161–176, 1996. 4278

Sicard, M., Perez, C., Rocadenbosch, F., Baldasano, J., and García-Vizcaino, D.: Mixed-Layer Depth Determination in the Barcelona Coastal Area from Regular Lidar Measurements: Methods, Results and Limitations, Bound.-Lay. Meteorol., 119, 135–157, doi:10.1007/s10546-005-9005-9, 2006. 4278

Sorbjan, Z.: Structure of the atmospheric boundary layer, Prentice Hall, Engelwood Cliffs, New Jersey, USA, 1989. 4279

Souch, C. and Grimmond, S.: Applied climatology: urban climate, Progress in Physical Geography, 30, 270–279, doi:10.1191/0309133306pp484pr, 2006. 4277

Steyn, D., Baldi, M., and Hoff, R.: The detection of mixed layer depth and entrainment zone thickness from lidar backscatter profiles, J. Atmos. Ocean. Tech., 16, 953–959, doi:10.1175/1520-0426(1999)016<0953:TDOMLD>2.0.CO;2, 1999. 4278

Stull, R. B.: An Introduction to Boundary Layer Meteorology, Kluwer Academic Publishers, Dordrecht, the Nederlands, 1988. 4277, 4290

Taylor, G.: Diffusion by continous movements, P. Lond. Mathemat. Soc., 20, 196–212, doi:10.1112/plms/s2-20.1.101, 1922. 4285

Taylor, G.: Statistical theory of turbulence part I–IV, P. Roy. Soc. Lond., 151, 421–478, doi:10.1098/rspa.1935.0158, 1935. 4285





AMTD
7, 4275–4319, 2014



Träumner, K.: Einmischprozesse am Oberrand der konvektiven atmosphärischen Grenzschicht, Ph.D. thesis, Fakultät für Physik des Karlsruher Instituts für Technologie (KIT), Karlsruhe, http://www.imk-tro.kit.edu/4328_4862.php, 2010. 4285, 4291

Träumner, K., Kottmeier, C., Corsmeier, U., and Wieser, A.: Convective Boundary-Layer Entrainment: Short Review and Progress using Doppler Lidar, Bound.-Lay. Meteorol., 141, 369–391, doi:10.1007/s10546-011-9657-6, 2011. 4279, 4280, 4285, 4289, 4297

Tucker, S. C., Senff, C. J., Weickmann, A. M., Brewer, W. A., Banta, R. M., Sandberg, S., P., Law, D. C., and Hardesty, R. M.: Doppler Lidar Estimation of Mixing Height Using Turbulence, Shear, and Aerosol Profiles, J. Atmos. Sci., 26, 673–688, doi:10.1175/2008JTECHA1157.1, 2009. 4279, 4285

Vaisala: Ceilometer CT25K User's Guide, Helsinki, Finland, 1999. 4281

Van de Wiel, B. J. H., Moene, A. F., Hartogensis, O. K., De Bruin, H. A. R., and Holtslag, A. A. M.: Intermittent Turbulence in the Stable Boundary Layer over Land, Part III: A Classification for Observations during CASES-99, J. Atmos. Sci., 60, 2509–2522, doi:10.1175/1520-0469(2003)060<2509:ITITSB>2.0.CO;2, 2003. 4296

Weitkamp, C.: Lidar: Range-Resolved Optical Remote Sensing of the Atmosphere, Springer Series in Optical Sciences, Springer, New York, 2005. 4278

White, J. M., Bowers, J. F., Hanna, S. R., and Lundquist, J. K.: Importance of Using Observations of Mixing Depths in order to Avoid Large Prediction Errors by a Transport and Dispersion Model, J. Atmos. Ocean. Tech., 26, 22–32, doi:10.1175/2008JTECHA1134.1, 2009. 4277, 4298

Wiegner, M. and Geiß, A.: Aerosol profiling with the Jenoptik ceilometer CHM15kx, Atmos. Meas. Tech., 5, 1953–1964, doi:10.5194/amt-5-1953-2012, 2012. 4282

Wood, C., Järvi, L., Kouznetsov, R., Nordbo, A., Drebs, A., Vihma, T., Hirsikko, A., Suomi, I., Fortelius, C., O'Connor, E., Haapanala, S., Moilanen, J., Kangas, M., Karppinen, A., Joffre, S., Vesala, T., and Kukkonen, J.: An overview of Helsinki UrBAN, Sci. Total Environ., accepted, 2013. 4296

Xie, S., McCoy, R. B., Klein, S. A., Cederwall, R. T., Wiscombe, W. J., Jensen, M. P., Johnson, K. L., Clothiaux, E. E., Gaustad, K. L., Long, C. N., Mather, J. H., McFarlane, S. A., Shi, Y., Golaz, J.-C., Lin, Y., Hall, S. D., McCord, R. A., Palanisamy, G., and Turner, D. D.: ARM climate modeling best estimate data, B. Am. Meteorol. Soc., 91, 13–20, doi:10.1175/2009BAMS2891.1, 2010. 4294





AMTD
7, 4275–4319, 2014



**Table 1.** Comparison of the performance of the Vaisala CT25K and Jenoptik CHM15k ceilometers. $E$ is energy, noise factor is the square root of the number of pulses per profile, i.e. a measure for the increase in signal to noise ratio due to averaging over many pulses for one backscatter profile. The reduced backscatter is calculated from the wavelength using $\nu_{mie} = 1.4$.

| | CT25K | CHM15k | CHM15k/CT25K | CHM15k feature |
|---|---|---|---|---|
| Wavelength (nm) | 905 | 1064 | 1.18 | less energy per photon |
| $E$/pulse (µJ) | 1.6 | 8 | 5.00 | more power |
| Pulses/profile | 65 536 | 105 650 | 1.61 | more pulses |
| Aperture ($m^2$) | 0.0165 | 0.0154 | 0.93 | smaller aperture |
| Range gate length | 30 | 15 | 0.50 | shorter gates |
| Mie backscatter (A. U.) | 7.26 | 5.78 | 0.80 | less backscatter |
| Noise factor | 256 | 325 | 1.27 | better noise reduction |
| Emitted photons | | | 9.48 | more emitted |
| Received photons | | | 4.42 | more received |





AMTD
7, 4275–4319, 2014



**Table 2.** Statistical measures for the intercomparison of the 5 min $MLH_{aero}$ and $MLH_{wind}$ time series. Given are slope, offset (Ofs.) and the regression coefficient ($R$) from a linear fit as well as bias and root mean square error (RMSE).

| | All data | | | | Cloudy excluded | | | |
|---|---|---|---|---|---|---|---|---|
| | MAM | JJA | SON | DJF | MAM | JJA | SON | DJF |
| Slope | 0.40 | 0.34 | 0.46 | 0.21 | 0.29 | 0.34 | 0.63 | 0.22 |
| Ofs. (km) | 0.68 | 0.89 | 0.59 | 0.45 | 0.91 | 0.99 | 0.58 | 0.71 |
| $R$ | 0.43 | 0.35 | 0.43 | 0.26 | 0.32 | 0.36 | 0.50 | 0.20 |
| Bias (km) | 0.16 | 0.22 | 0.22 | −0.07 | 0.22 | 0.30 | 0.35 | 0.17 |
| RMSE (km) | 0.64 | 0.68 | 0.54 | 0.52 | 0.68 | 0.66 | 0.52 | 0.66 |





AMTD
7, 4275–4319, 2014



**Table 3.** Comparison of the capabilities of the MLH retrievals in different situations. Abbreviations are: AL = aerosol layer, ML = mixed layer, NBL = nocturnal boundary layer, RL = residual layer.

| Situation | Ceilometer | | Wind lidar | |
|---|---|---|---|---|
| Night | −− | detects AL's, NBL or top of RL | + | intermittent turbulence? |
| Growing ML | ∘ | no gradient between ML and RL | ++ | clear difference between ML and RL |
| Fully developed ML | ++ | top of ML coincides with top of AL | ++ | strong turbulence over whole ML |
| Evening decay | − | sticks to top of aerosol layer | + | sees decaying mixing |





AMTD
7, 4275–4319, 2014



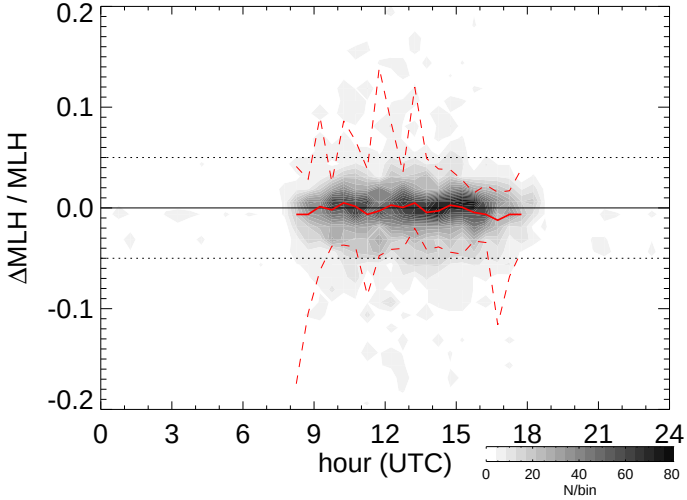


**Fig. 1.** Relative difference $(MLH_{CT25K} - MLH_{CHM15k})/MLH_{CHM15k}$ of retrieved $MLH_{aero}$ from Vaisala CT25K and Jenoptik CHM15k as function of time of the day for the period 16 August–16 November 2013. Shading shows histogram of single retrievals with a bin size of 30 min and 0.0125 (1.25 %) relative MLH change. Red lines are the 25 and 75 % percentile (dashed) and the median (solid) of half hour intervals, respectively. In total 9173 data points were analysed. During daytime there were in average 80 % of the original data per half hour interval available. During times when less than 20 % of the original data were available median and quartiles are not displayed. Dotted lines mark ±0.05 chosen as the average error for the $MLH_{aero}$ estimate.





AMTD
7, 4275–4319, 2014



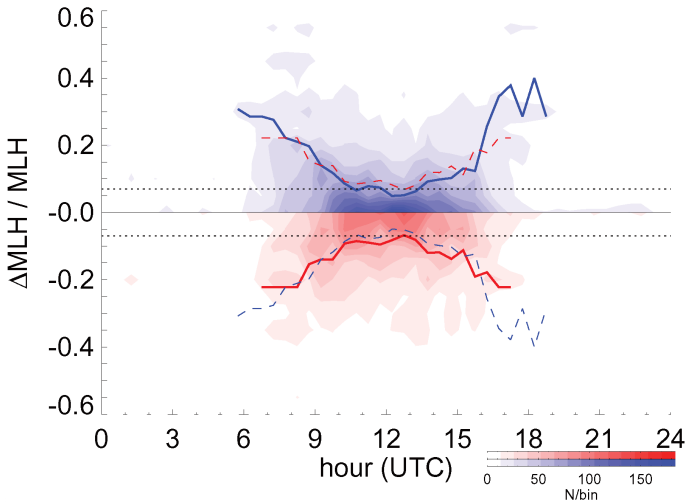


**Fig. 2.** Relative change $\Delta\mathrm{MLH}/\mathrm{MLH} = (\mathrm{MLH}_{\pm} - \mathrm{MLH}_{0.4})/\mathrm{MLH}_{0.4}$ of retrieved $\mathrm{MLH}_{\pm}$ for $\sigma_{\mathrm{wts}} = (0.4 \pm 0.1)\,\mathrm{ms}^{-1}$ as a function of time of the day. Shading gives the histogram for single retrievals with $\sigma_{\mathrm{wts}}$ increased (red) and decreased (blue). Bin size is 30 min and 0.05 (5 %) relative MLH change. Solid lines are half hour medians for increase (red) and decrease (blue) of $\sigma_{\mathrm{wts}}$, respectively. Dashed lines are medians mirrored at zero. A total of 8667 (11 218) records have been used for the upper (lower) histogram. During daytime there are in average 440 out of 540 points per half hour interval. Medians are not shown for times when less than 20 % of the original data gave an estimate Horizontal black dotted lines indicate the ±7 % change derived from the $\sigma_w$ profile of Lenschow et al. (1980).





AMTD
7, 4275–4319, 2014

MLH from ceilometer and wind lidar

J. H. Schween



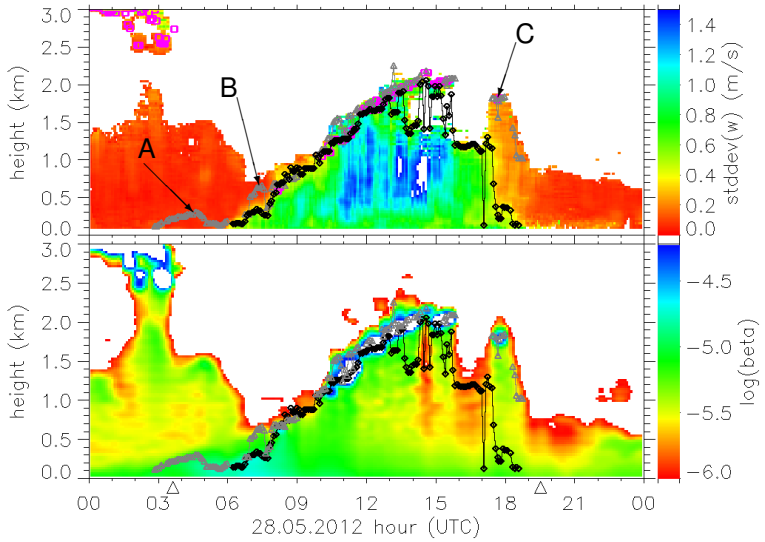


**Fig. 3.** Time height sections of standard deviation of the vertical velocity (stddev, top panel) and aerosol backscatter coefficient (beta, bottom panel) on 28 May 2012. MLH retrieved from wind lidar (solid black with diamonds) and from ceilometer (solid grey with triangles). Magenta squares indicate cloud base heights as determined by the ceilometer. Triangles at the abscissa mark sunrise and sunset. Letters A, B and C refer to descriptions in the text.





AMTD
7, 4275–4319, 2014



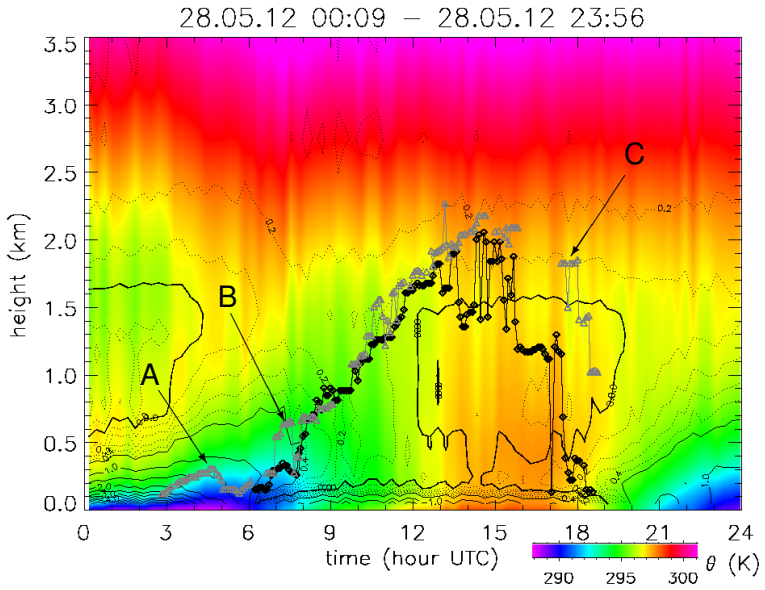


**Fig. 4.** Time height section of potential temperature from HATPRO (color shading). Black lines with diamonds shows ML from wind, grey line with triangle ML from aerosol. Solid isolines show the vertical potential temperature gradient in steps of 0.5 K/100 m (solid), dotted lines in steps of 0.1 K/100 m between −0.9 K/100 m to +0.9 K/100 m. The thick isoline marks neutral stratification (0 K/100 m). Letters A, B and C refer to descriptions in the text.





AMTD
7, 4275–4319, 2014



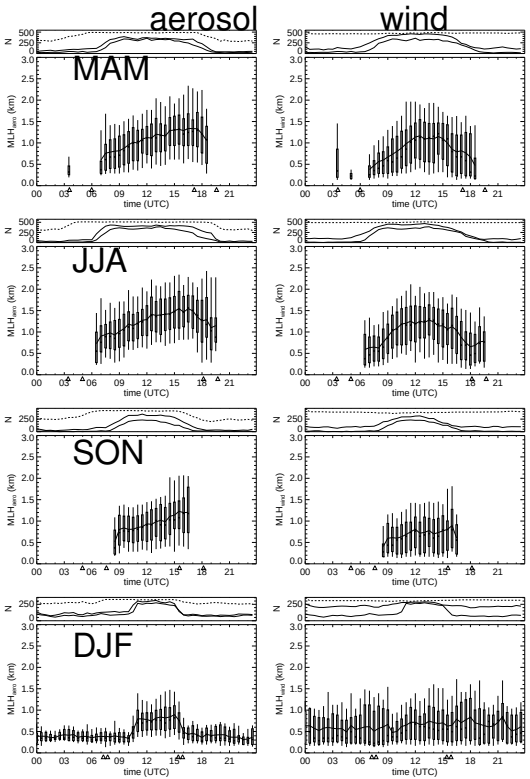


**Fig. 5.** Average diurnal course (solid line) of MLH from aerosol (left panels) and vertical wind (right panels) for spring (MAM), summer (JJA), autumn (SON) and winter (DJF). Whiskers and boxes indicate 10, 25, 75 and 90 % percentiles. The center dot indicates the median. On top of every subplot the number of cases *N* is shown before excluding any data (dashed), after excluding data from the respective instrument (solid thin line) and after synchronizing with the other instrument (solid thick). Triangles at the abscissa mark range of sunset and sunset during the respective season.





AMTD
7, 4275–4319, 2014





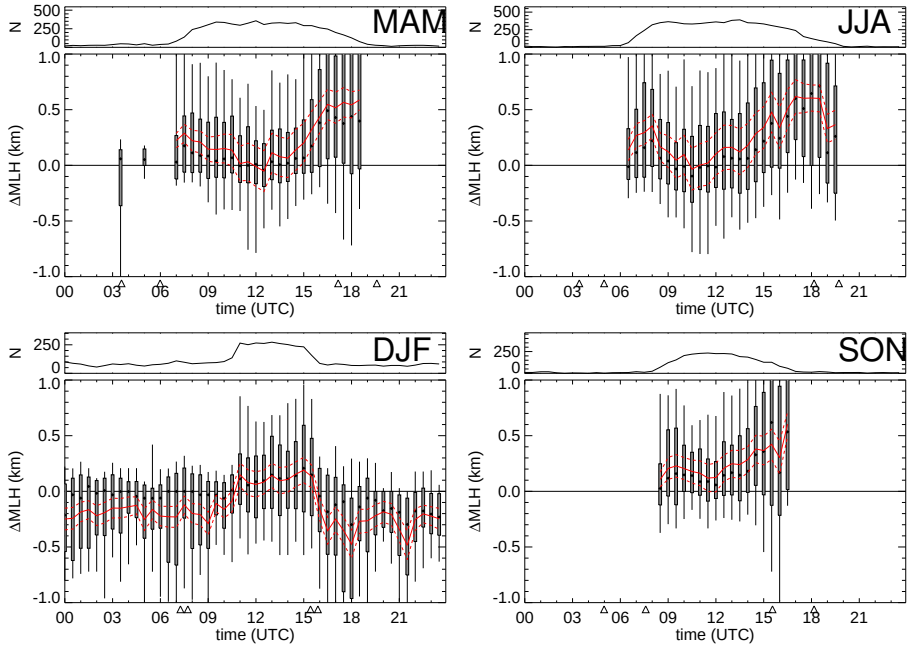


**Fig. 6.** Difference $\Delta MLH = MLH_{aero} - MLH_{wind}$ for the four seasons. Whiskers and boxes indicate 10, 25, 75 and 90 % percentiles and dots indicate the median. Red lines indicate average (solid) and the error estimate based on the sensitivity studies in Sects. 2.1.4 and Sect. "Threshold sensitivity" (dashed).





AMTD
7, 4275–4319, 2014



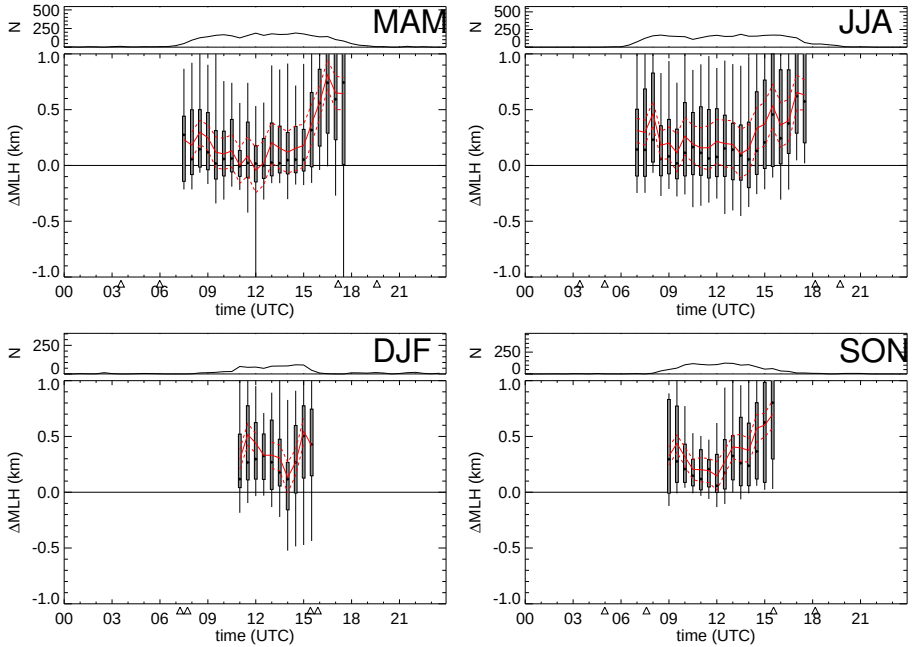


**Fig. 7.** As Fig. 6 but with cloudy cases excluded.





AMTD
7, 4275–4319, 2014

MLH from ceilometer and wind lidar

J. H. Schween



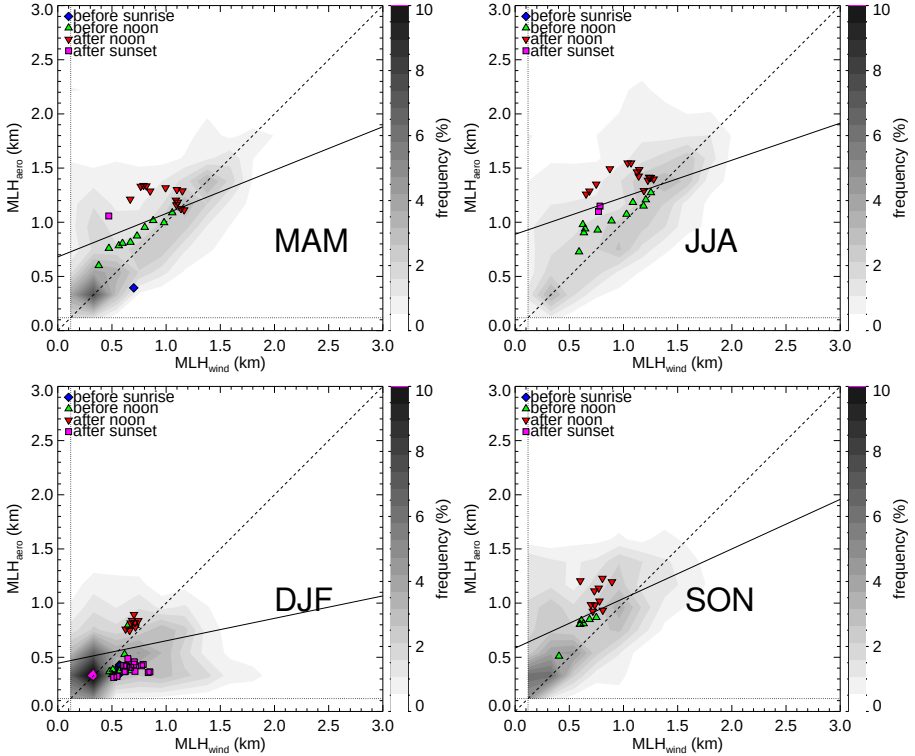


**Fig. 8.** Joint histograms of MLH from wind lidar (abscissa) and ceilometer (ordinate) for (clock wise from top left) spring (MAM), summer (JJA), autumn (SON) and winter (DJF). Binsize of the histograms is 210 m starting at 120 m. Colored symbols show average diurnal course for times before sunrise (blue diamonds), before noon (green triangles pointing upwards), afternoon (red triangles pointing downwards) and after sunset (magenta squares). Straight lines are linear regressions fitted to every data pair.





AMTD
7, 4275–4319, 2014



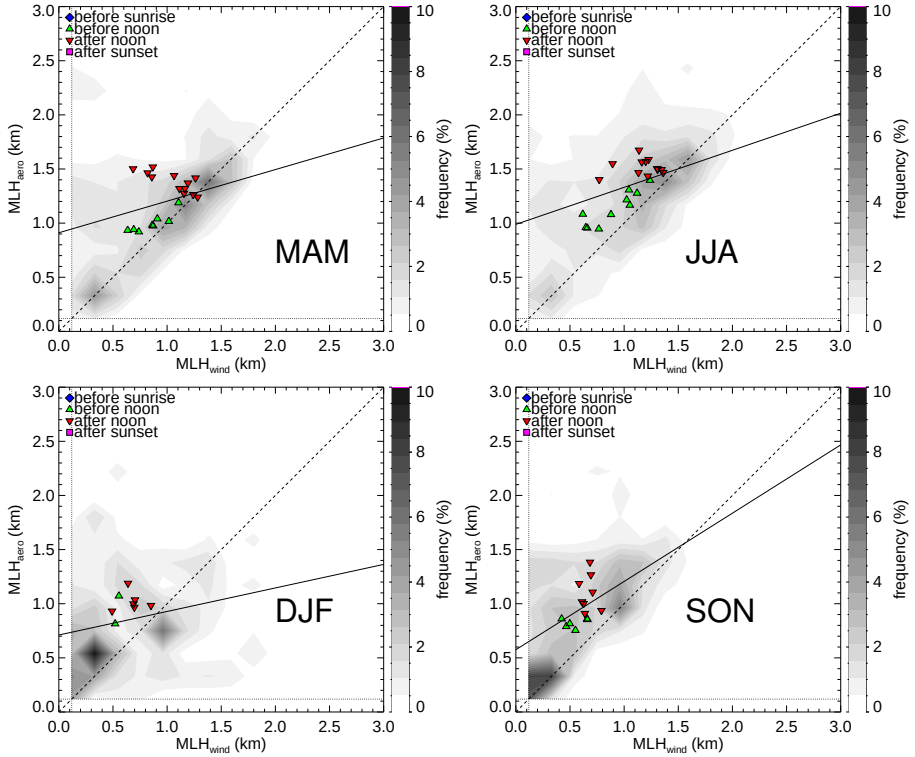


**Fig. 9.** As Fig. 8 above but with cloudy cases excluded.





AMTD
7, 4275–4319, 2014



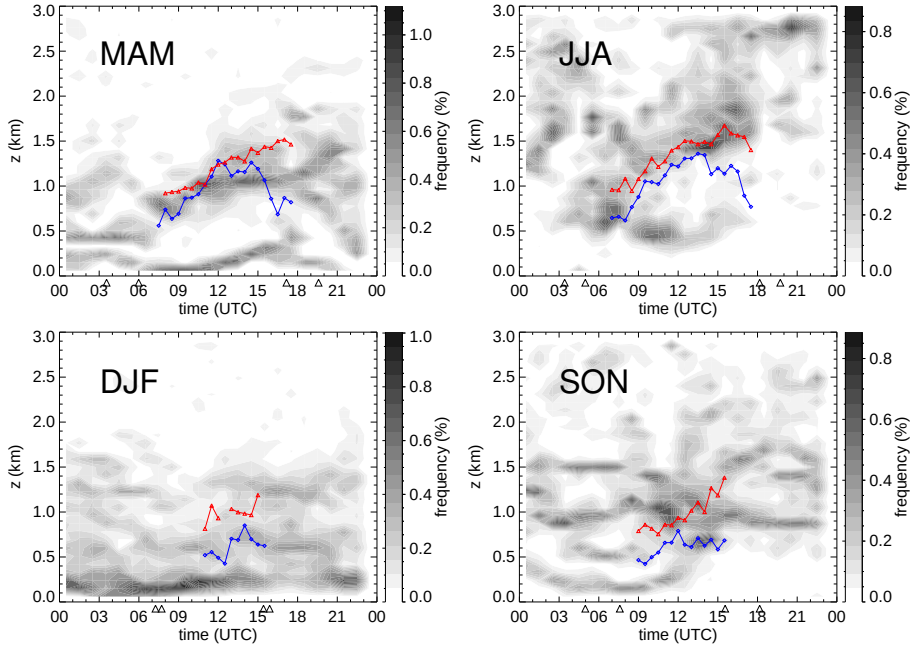


**Fig. 10.** Histogram of cloud bases (shading) and overlayed ML from aerosol (red) and wind (blue) with cloudy cases excluded. Bin size is 90 m × 1 h. Cloud base heights from half hour intervals when cloud coverage was larger than 4 octa are excluded.





AMTD
7, 4275–4319, 2014